



NLRP3 deficiency did not attenuate NASH development under high fat calorie diet plus high fructose and glucose in drinking water

Liu-Yan Zhu¹ · Chang Liu¹ · Zong-Rui Li¹ · Chen Niu¹ · Jian Wu^{1,2,3}

Received: 2 November 2020 / Revised: 21 December 2020 / Accepted: 22 December 2020 / Published online: 1 February 2021
© The Author(s), under exclusive licence to United States and Canadian Academy of Pathology 2021

Abstract

NOD-like receptor protein 3 (NLRP3) promotes the inflammatory response during progression of nonalcoholic fatty liver (NAFL) to nonalcoholic steatohepatitis (NASH). This study aimed to further delineate the role of NLRP3 in NASH development by abolishing its expression in mice. A high-fat and calorie diet plus high fructose and glucose in drinking water (HFCD-HF/G) was used to establish NASH in both wild-type (WT) and NLRP3 knock-out (KO) mice. Hepatocellular injury, hepatic steatosis and fibrosis, as well as inflammatory response and insulin resistance in the liver and epididymal white adipose tissue (eWAT) were determined. Elevated body weight, liver weight and serum alanine transaminase level, increased hepatic triglyceride accumulation and collagen deposition, and worsened systemic insulin resistance were observed in *Nlrp3*^{-/-} mice compared to WT mice under HFCD-HF/G feeding. Upregulated hepatic transcription of tumor necrosis factor- α (TNF- α) and monocyte chemoattractant protein-1 (MCP-1), and enhanced infiltration of inducible nitric oxide synthase-positive (iNOS⁺) M1 macrophages were also documented in HFCD-HF/G-fed *Nlrp3*^{-/-} mice in comparison to HFCD-HF/G-fed WT mice. Moreover, transcription of TNF- α and MCP-1 and infiltration of iNOS⁺ M1 macrophages were increased in the liver of *Nlrp3*^{-/-} mice under control diet. NLRP3 deficiency did not attenuate, but instead aggravated NASH development under HFCD-HF/G feeding. The worsened extent of NASH might be attributed to enhanced hepatic MCP-1 expression and M1 macrophage infiltration in *Nlrp3*^{-/-} mice. Our study points to additional caution when NLRP3 blockade is considered as a therapeutic strategy in the treatment of human NASH.

Introduction

Nonalcoholic fatty liver disease (NAFLD) is the deposition of fat in hepatocytes without excessive alcohol consumption or other conditions leading to steatosis. Recognized as the hepatic manifestation of obesity-related metabolic

syndrome, NAFLD is increasingly prevalent and represents an emerging global healthcare challenge [1, 2]. Fatty liver is histologically defined as the presence of more than 5% of steatotic hepatocytes, and NAFLD ranges from nonalcoholic fatty liver (NAFL) to nonalcoholic steatohepatitis (NASH) and even cirrhosis or hepatocellular carcinoma (HCC) [3–5]. Characterized by varying degrees of steatosis, inflammation, hepatocellular ballooning and fibrotic change, NASH is seen as the active form of NAFLD [6]. However, the underlying pathogenesis of NASH development has not been fully understood. A “multi-hits” hypothesis is widely accepted to explain the evolution with lipotoxicity, chronic inflammation, insulin resistance and adipose tissue dysfunction being the key factors [7].

Inflammasomes are a group of protein complexes responsible for caspase-1-dependent maturation and release of IL-1 β and IL-18 [8]. As a member of the inflammasome family, NOD-like receptor protein 3 (NLRP3) is activated in a variety of inflammatory immune responses [9], and has been implicated in multiple sterile inflammatory diseases, such as gout, atherosclerosis, type 2 diabetes, Alzheimer’s

Supplementary information The online version contains supplementary material available at <https://doi.org/10.1038/s41374-021-00535-3>.

✉ Jian Wu
jian.wu@fudan.edu.cn

- ¹ Department of Medical Microbiology and Parasitology, MOE/NHC/CAMS Key Laboratory of Medical Molecular Virology, School of Basic Medical Sciences, Fudan University Shanghai Medical College, Shanghai 200032, China
- ² Department of Gastroenterology & Hepatology, Zhongshan Hospital of Fudan University, Shanghai 200032, China
- ³ Shanghai Institute of Liver Diseases, Fudan University Shanghai Medical College, Shanghai 200032, China

disease, and liver disorders [10]. A substantial body of literature supported the critical role of NLRP3 in the mediation of inflammation and insulin resistance during NAFLD progression based on the fact that NLRP3 expression was significantly increased in both murine models and humans with NASH [11–14], while its inhibition improved the pathologic abnormalities [15, 16]. However, contradictory findings indicated that NLRP3 deficiency may not always be beneficial for the development of NASH [17–19].

The present study aimed to further investigate the role of NLRP3 in NASH development. A well-characterized high fat calorie diet plus high fructose and glucose in drinking water (HFCD-HF/G)-induced murine model that could recapitulate histologic and metabolic features of human NASH with fibrosis [20] was used to determine whether NLRP3 deficiency would attenuate or aggravate the development of NASH. Given the crucial role of white adipose tissue (WAT) in NAFLD [21, 22], insulin resistance and inflammatory status in epididymal WAT (eWAT) were also investigated. The results suggested that NLRP3 deficiency aggravated NASH development including fibrotic progression under HFCD-HF/G feeding. Increased expression of monocyte chemoattractant protein-1 (MCP-1) and enhanced infiltration of inducible nitric oxide synthase-positive (iNOS⁺) M1 macrophages in the liver might account for the worsened NASH pathology in *Nlrp3*^{-/-} mice. Our study underscores the potentially detrimental effect of NLRP3 inhibitory therapy which is considered as a strategy in the clinical management of NASH.

Materials and methods

Animals and diets

Male wild-type (WT) and *Nlrp3*^{-/-} (B6.129S6-*Nlrp3*^J; Stock 021302) C57BL/6 mice originated, respectively, from Biomedical Research Institute of Nanjing University (Nanjing, China) and Jackson Laboratory (ME, USA). All mice were housed under a specific pathogen-free condition with 12-hrs light/dark cycle at 22 °C in the Experimental Animal Center, Fudan University (Shanghai, China). A murine model of NASH was established as previously described [20]. At 10 weeks of age, both WT and *Nlrp3*^{-/-} mice were assigned to either a control diet (#1010010; XIETONG ORGANISM, China), or a high fat calorie diet (D12492i; Research Diets, USA) plus high fructose (23.1 g/L; F3510, Sigma, USA) and glucose (18.9 g/L; G8270, Sigma, USA) in drinking water (HFCD-HF/G). Thus, mice were randomly divided into four groups (n = 3 per group): WT-CD, WT-HFCD-HF/G, *Nlrp3*^{-/-}-CD and *Nlrp3*^{-/-}-HFCD-HF/G. Body weight of each group was recorded weekly during 16 weeks of feeding. Animal experiments were performed

following the NIH guidelines with experimental protocols approved by the Animal Ethic Committee of Fudan University School of Basic Medical Sciences.

Genotype identification

Mouse tail tissue was lysed overnight in Tris-HCl buffer (5 mM EDTA, 400 mM NaCl, 1% SDS, 0.1 mg/ml Proteinase K) with water bath at 55 °C. Phenol-chloroform (1:1) of equal volume to the lysate was added and mixed thoroughly to extract genomic DNA. The mixture was then centrifuged (12,000 g for 15 min) to pellet tissue debris, and the upper liquid phase was transferred to mix with 100% ethanol and rested at -20 °C for ≥2 hrs. Thereafter, centrifugation was conducted again to precipitate DNA and remove the supernatant. The DNA was washed in 70% ethanol, centrifuged and air-dried, and fully dissolved in sterile ddH₂O. DNA at 500 ng was used as template in each PCR reaction containing Taq mix (KT201; TIANGEN, China). Amplification was performed using a gradient thermal cycler (T100; Bio-Rad; USA), and the PCR products were electrophoresed (HE-120; Tanon, China), and visualized (14T5561-1159; Tanon, China) in agarose gel. The primers used include:

Mutant forward: 5'-TGCCTGCTCTTTACTGAAGG-3',

Wild-type forward: 5'-TCAGTTTCCTTGGCTACCA GA-3' and

Common reverse: 5'-TTCCATTACAGTCACTCCAGA TGT-3'.

Intraperitoneal glucose tolerance test

Intraperitoneal glucose tolerance test (IGTT) was performed 3 days before mice were sacrificed. Body weight and the fasting blood glucose levels were recorded after they were fasted overnight for 15 h. Mice were injected intraperitoneally with sterile D-glucose (V900392; Sigma, USA) solution at 2.5 g/kg body weight. Blood glucose was measured 30, 60, 90, and 120 min after intraperitoneal injection using a glucometer (HGM-112; Omron, China). Area under each curve of IGTT was calculated. Mice were sacrificed humanely and tissue samples were harvested and stored at -80 °C until analysis.

Serological analysis

Serum was obtained after centrifuging (1000 × g for 10 min at 4 °C) blood collected from mouse eye orbit. Serum levels of triglyceride (TG), total cholesterol (TC), low-density lipoprotein cholesterol (LDL-C), high-density lipoprotein cholesterol (HDL-C), and alanine aminotransferase (ALT) were determined by an automated biochemical analyzer (AU680; Beckman Coulter, USA).

Liver histopathologic examination

The paraffin-embedded liver tissue was cut into 4 μm -thick sections for hematoxylin and eosin (H&E) staining or Masson trichrome staining. Histopathologic examination was performed in single-blinded fashion by a board-certified pathologist. Kleiner classification [23] was employed to establish NAFLD activity score (NAS; 0–8) in sections with H&E staining, including steatosis (0–3), lobular inflammation (0–3), and hepatocellular ballooning (0–2). NASH was defined if $\text{NAS} \geq 5$. Hepatic collagen deposition was assessed through Masson staining with the positive blue area quantified by Image J (NIH, USA). All sections were scanned into digital images and several view fields (≥ 3) of each section were captured respectively in H&E (K-Viewer; KFBIO, China) and Masson trichrome staining (CaseViewer; 3DHISTECH, Hungary).

Quantitative real-time PCR

Liver or eWAT tissue was homogenized and lysed in TRIzol (#15596018, Life Technologies, USA) to isolate total RNA following the manufacturer's instructions. RNA at 500 ng was reversely transcribed to cDNA with a Primer-Script RT kit (RR037A; Takara, Japan). Quantitative real-time PCR was monitored by TB Green Premix (RR420A; Takara, Japan) on a realplex4 mastercycler (AG22331; Eppendorf, Germany). Melting curve analysis was employed to determine the specificity of amplification. Relative gene transcription level was calculated using $\Delta\Delta\text{CT}$ method with 18 S rRNA being the house-keeping gene [24]. Primers used are listed in Supplemental Table S1.

Immunoblot analysis

Protein was extracted with RIPA lysis buffer (P0013B; Beyotime Biotechnology, China) and quantified using BCA method. Heat-denatured protein at 40 μg was loaded per lane, separated by SDS-PAGE electrophoresis, transferred onto polyvinylidene fluoride (PVDF) membrane (IPVH00010; Millipore, USA). The membrane was blocked in 5% non-fat milk (A600669; Sangon Biotech, China) at room temperature for 1 h and probed with primary antibodies at 4 °C overnight. After being washed in 0.1% Tris-buffered saline (TBS) plus Tween 20, the membrane was incubated at room temperature for 1 h with horseradish peroxidase-conjugated secondary antibodies. Image of the membrane was developed using an ECL kit (E412-01; Vazyme, China) followed by exposure in a chemiluminescent imaging instrument (14T12NPFLI6-348; Tanon, China), and the densitometry was analyzed by Image J. Antibodies used are listed in Supplemental Table S2.

Immunofluorescent staining

Frozen liver sections were dried at room temperature, fixed in 4% paraformaldehyde for 15 min, and then washed with TBS/0.03% Triton X-100. Antigen retrieval was achieved by soaking sections in pH 6.0 sodium citrate buffer for 20 min at 90 °C [25, 26]. Thereafter, tissues on the sections were blocked at room temperature for 1 h with 5% goat serum (SL038; Solarbio, China) in TBS/1% bovine serum albumin, followed by incubation with primary antibodies of inducible nitric oxide synthase (iNOS) (1:50; sc-7271, Santa, USA) or CD163 (1:50; sc-58965, Santa, USA), and CD68 (1:200; BA3638, BOSTER, China) at 4 °C overnight. After being washed, tissue sections were incubated in dark with Alexa Fluor 488 or 594-conjugated secondary antibodies (1:400; A21202/A21207, Invitrogen, USA) at room temperature for 1 h. Nuclei were counterstained with 4',6-diamidino-2-phenylindole (DAPI; C1005, Beyotime Biotechnology, China). All sections were sealed with antifade mounting medium (G1401; Servicebio, China) and viewed under a confocal microscope (TCS SP8; Leica, Germany) with four visual fields of each tissue randomly captured. Different fluorescent area was quantified using Image J and normalized by nucleus number.

Hepatic triglyceride determination

Liver tissue was homogenized (SKSI; Biheng Biotechnology, China) to determine triglyceride (TG) level with a kit (E1013; Applygen Technologies, China). A multi-mode microplate reader (FlexStation 3; Molecular Devices, USA) was used to measure the absorbance at 550 nm. TG content was corrected with protein concentration determined by BCA method (#23227; Thermo, USA).

Statistical Analysis

All data presented as mean \pm SD were analyzed with GraphPad prism V.7.0. One or two-way ANOVA in combination with uncorrected Fisher's LSD test was used for comparisons of quantitative variables showing normal distribution. Kruskal–Wallis with uncorrected Dunn's post-hoc test was used in nonparametric data analysis. Statistical significance level was set at a p value of 0.05 with $*p < 0.05$, $**p < 0.01$ and $***p < 0.001$ versus respective control.

Results

Genotyping and expression of NLRP3 in different mouse groups

B6.129S6-*Nlrp3*^J-021302 knock-out mice were established with a neo cassette replacing the entire NLRP3 coding

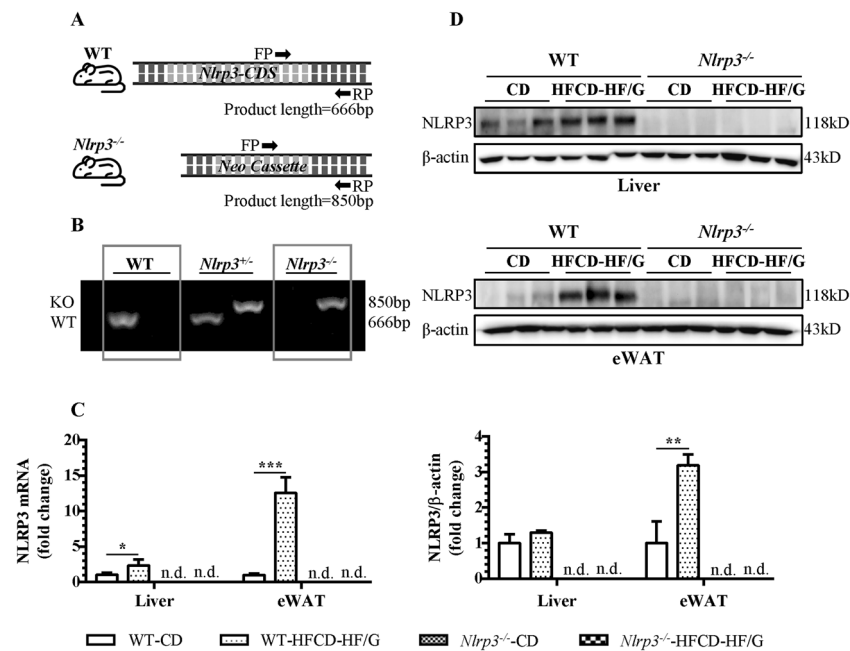


Fig. 1 Genotyping and NLRP3 expression in different mouse groups. **A, B.** In B6.129S6-Nlrp3/J-021302 knock-out mice, the coding sequence (CDS) of NLRP3 is replaced by neo cassette. Different forward primers (FP) and same reverse primer (RP) were used in genotyping (**A**). DNA gel electrophoresis showed the amplified products of two primer pairs with 850 bp of knock-out (KO) band while

666 bp of wild-type (WT) band. Homozygous WT and *Nlrp3*^{-/-} mice were taken into this study (**B**). **C** NLRP3 mRNA level in the liver and eWAT. **D** NLRP3 protein expression in the liver and eWAT were measured by immunoblotting and quantified by image J. Both mRNA and protein of NLRP3 were not detected (n.d.) in two *Nlrp3*^{-/-} groups.

sequence to abolish its expression. Genotypes of all experimental mice were identified at first with different forward primers and same reverse primer (Fig. 1A). Amplified products were limited to 666 bp and 850 bp respectively in wild-type (WT) and knock-out (KO) mice as exemplified (Fig. 1B). NLRP3 expression in both liver and eWAT was examined upon sample collection. At a transcription level, HFCD-HF/G-fed WT mice showed moderate (twofold) upregulation of NLRP3 in the liver and much more pronounced (12-fold) in eWAT compared to control diet-fed WT mice. NLRP3 mRNA was not detected in either *Nlrp3*^{-/-} group (Fig. 1C). NLRP3 protein was relatively more expressed in the liver than eWAT of WT mice under control diet, however, its increase induced by HFCD-HF/G in eWAT was three times of that in the liver. As expected, NLRP3 protein was absent in both *Nlrp3*^{-/-} groups (Fig. 1D). These results demonstrated successful removal of the NLRP3 gene in knock-out mice and there was its differential expression between liver and eWAT in WT mice fed different diets.

NLRP3 deficiency aggravated body and liver fat deposition and hepatic injury under HFCD-HF/G feeding

Mice under control diet displayed a slow increase of body weight, while HFCD-HF/G feeding stimulated a remarkable

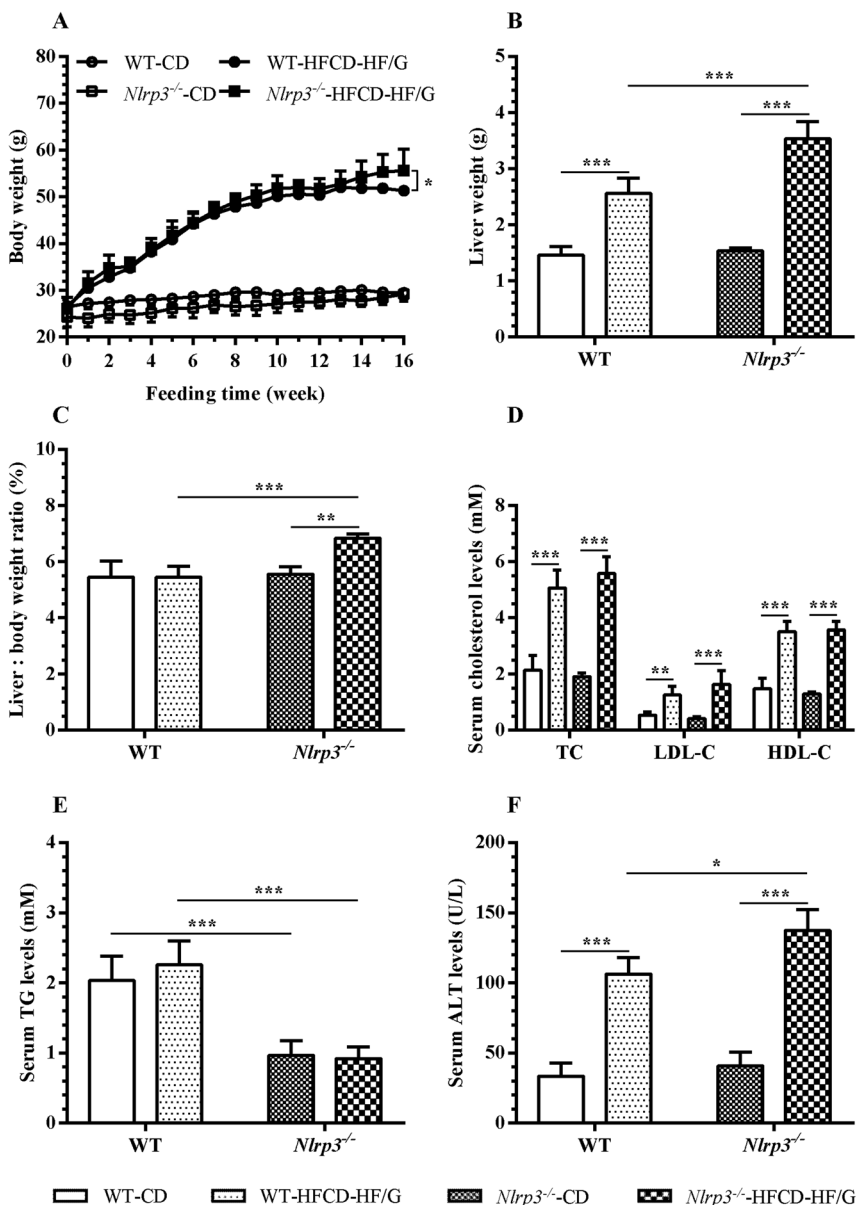
weight gain throughout the investigational period with WT mice reaching a plateau during the last 13–16 weeks while *Nlrp3*^{-/-} mice maintaining the uptrend (Fig. 2A). HFCD-HF/G feeding also significantly increased liver weight, which was more evident in *Nlrp3*^{-/-} mice concomitantly with an elevated liver/body weight ratio in comparison to WT mice (Fig. 2B, C). Despite notable increases induced by HFCD-HF/G compared to control diet, serum TC, LDL-C and HDL-C levels between two HFCD-HF/G groups showed no statistical differences (Fig. 2D). Interestingly, serum TG levels in both *Nlrp3*^{-/-} groups were much decreased compared with WT groups regardless of diets (Fig. 2E). Serum ALT level was significantly higher in *Nlrp3*^{-/-} mice than WT mice under HFCD-HF/G feeding, indicating a more serious liver injury existed in HFCD-HF/G-fed *Nlrp3*^{-/-} mice (Fig. 2F). In summary, NLRP3 deficiency aggravated body weight, liver fat deposition and hepatic injury under HFCD-HF/G feeding.

NLRP3 deficiency exacerbated hepatic steatosis and collagen deposition under HFCD-HF/G feeding

H&E staining of liver sections presented extensive hepatocellular ballooning and increased inflammatory infiltration in addition to steatosis in both HFCD-HF/G groups. NAFLD activity score (NAS) accordingly demonstrated that NASH (NAS ≥ 5) was established in the two groups.

Fig. 2 NLRP3 deficiency aggravated body and liver fat deposition and hepatic injury under HFCD-HF/G feeding.

Weight gain during 16 weeks of investigational period (A), liver weight (B) and liver/body weight ratio (C) in each mouse group. Serum cholesterol levels including total cholesterol (TC), low-density lipoprotein cholesterol (LDL-C) and high-density lipoprotein cholesterol (HDL-C) (D), as well as serum triglyceride (TG) level (E) and alanine aminotransferase (ALT) level (F).



HFCD-HF/G-induced macrovesicular steatosis tended to be more profound in *Nlrp3*^{-/-} mice than WT mice. Of note, *Nlrp3*^{-/-} mice had a statistically increased NAS compared to WT mice under control diet with inflammation index being the main difference (Fig. 3A, B). Based on the great elevation in hepatic TG level under HFCD-HF/G feeding, liver steatosis was more severe in *Nlrp3*^{-/-} mice than WT mice (Fig. 3C). Masson trichrome staining was employed to assess hepatic collagen deposition. Compared with control diet groups, blue-stained collagen fibrils which gathered into slim bundles that distributed in the liver parenchyma were remarkably increased in HFCD-HF/G groups. Furthermore, semiquantitative morphometric analysis of Masson-positive area showed that there was significantly more collagen deposition in the liver of both *Nlrp3*^{-/-}

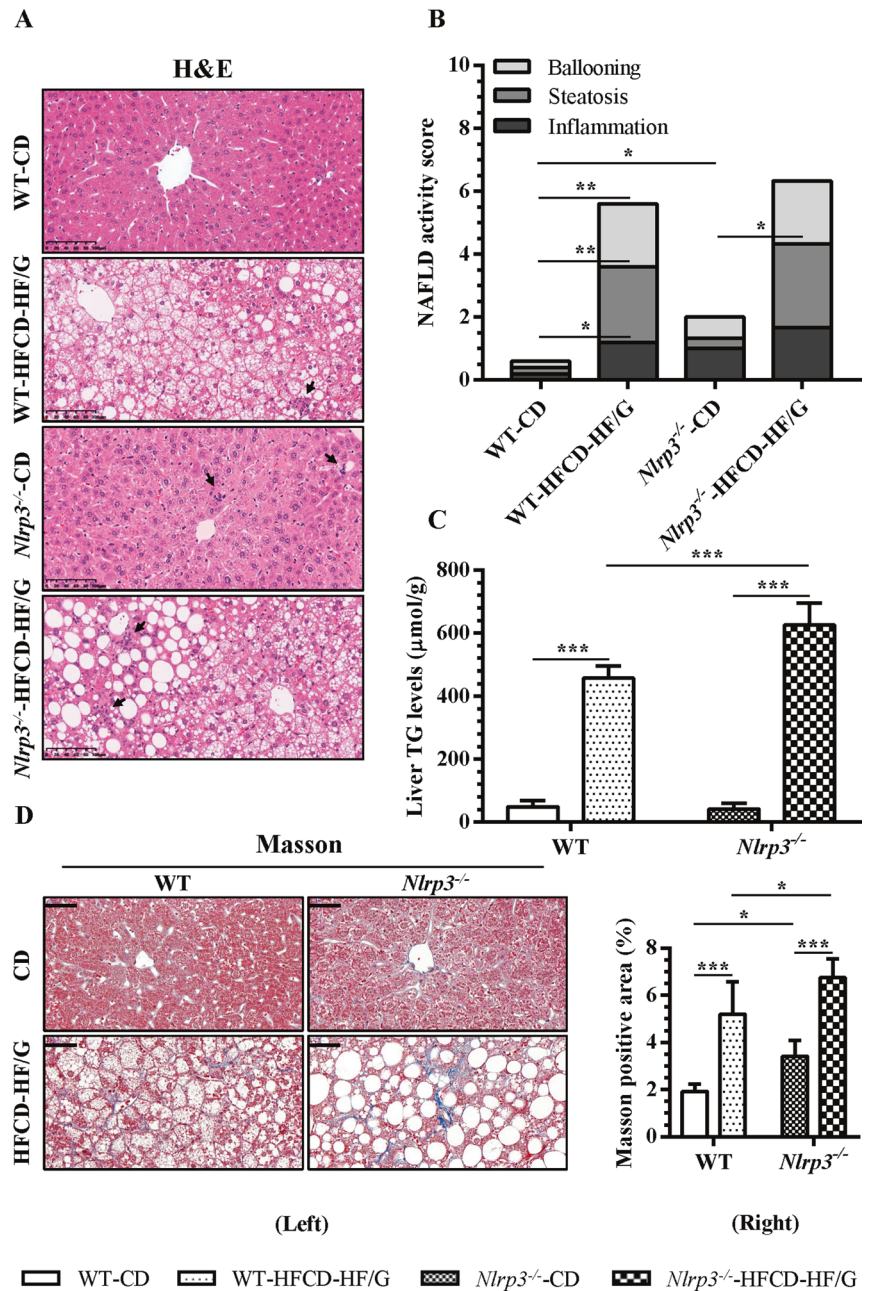
groups than corresponding WT group (Fig. 3D). In summary, NLRP3 deficiency exacerbated hepatic steatosis and collagen deposition under HFCD-HF/G feeding.

NLRP3 deficiency worsened systemic insulin resistance under HFCD-HF/G feeding

Being a common feature of NASH, insulin resistance was evaluated by IGTT. While normal insulin sensitivity was exhibited in both control diet groups, HFCD-HF/G feeding led to higher blood glucose levels at each time point after glucose overload in *Nlrp3*^{-/-} mice than WT mice. Area under curves of IGTT confirmed the relatively more blunted insulin sensitivity in HFCD-HF/G-fed *Nlrp3*^{-/-} mice than HFCD-HF/G-fed WT mice (Fig. 4A, B). As a key molecule that

Fig. 3 NLRP3 deficiency exacerbated hepatic steatosis and collagen deposition under HFCD-HF/G feeding. **A** Hematoxylin-eosin (H&E)

staining of liver sections with arrows indicating inflammatory infiltration. Magnification, 400 \times ; Scale bars, 100 μ m. **B** H&E staining results were semi-quantitatively scored by evaluating hepatocellular ballooning, steatosis and lobular inflammation using NAFLD activity score (NAS) system. **C** Liver triglyceride (TG) level. **D** Masson trichrome staining was used to assess hepatic collagen deposition (Left). Blue area showed the collagen fibrils and was quantified by image J (Right). Magnification, 600 \times ; Scale bars, 50 μ m.



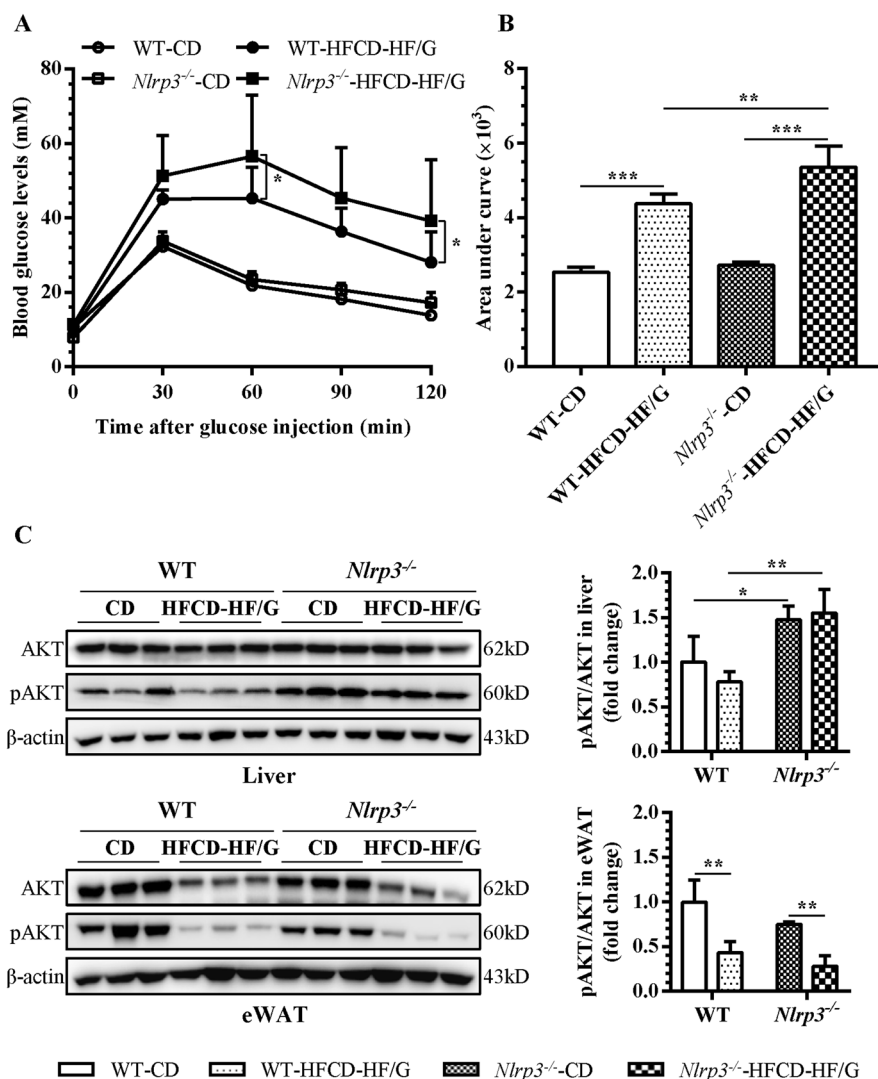
orchestrates diverse metabolic pathways including insulin receptor signaling, AKT requires phosphorylation of Ser473 to achieve its maximal activation [27]. Therefore, protein levels of AKT and its phosphorylation form pAKT-Ser473 were assayed in both liver and eWAT. AKT and pAKT-Ser473 levels together with the pAKT/AKT ratio in eWAT were generally declined in HFCD-HF/G groups in comparison to respective controls (Fig. 4C), implicating a severe disturbance of insulin signaling in adipose tissue. Surprisingly, hepatic pAKT-Ser473 and the pAKT/AKT ratio were significantly elevated in both *Nlrp3*^{-/-} groups compared with WT groups. In summary, NLRP3 deficiency further impaired

systemic insulin sensitivity under HFCD-HF/G feeding with prominent insulin resistance occurred in eWAT.

Transcription levels of TNF- α , MCP-1 and CD36 expression in the liver

As shown in Fig. 5, mRNA levels of two important inflammatory cytokines, TNF- α and MCP-1, were upregulated by HFCD-HF/G in both liver and eWAT regardless of mouse genotypes. Two cytokines especially MCP-1 in the liver displayed significantly higher transcription levels in *Nlrp3*^{-/-} mice than respective WT mice. Upregulated expression of

Fig. 4 NLRP3 deficiency worsened systemic insulin resistance under HFCD-HF/G feeding. **A** Intraperitoneal glucose tolerance test (IGTT) in each mouse group. **B** Area under curve of IGTT. **C** Protein levels of AKT and pAKT-Ser473 in the liver and eWAT were measured by immunoblotting and quantified by image J.

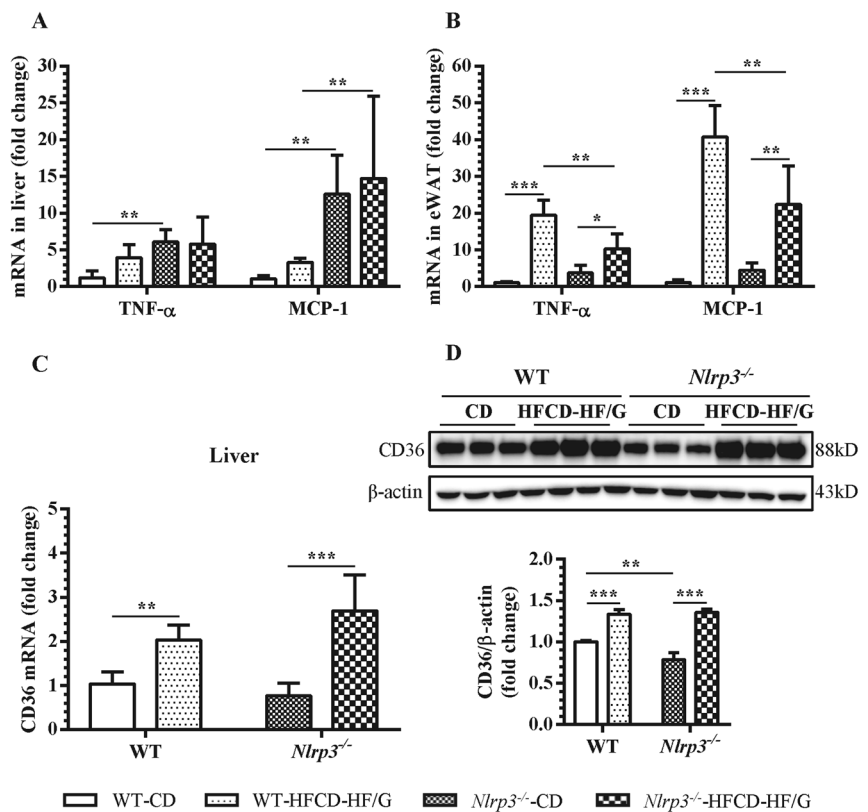


these inflammatory genes was more evident in eWAT compared to the liver in WT mice under HFCD-HF/G feeding. While HFCD-HF/G-fed *Nlrp3*^{-/-} mice showed significantly increased TNF- α and MCP-1 transcription in eWAT compared to control diet, the amplitude of upregulation was not as profound as HFCD-HF/G-fed WT mice (Fig. 5A, B). Hepatic CD36 expression is positively correlated with liver TG content and insulin resistance during NAFLD progression. To explore whether CD36 took a compensatory role for NLRP3 deficiency in this murine model of NASH, its expression in the liver was examined. Similar patterns of mRNA and protein expression were observed with prominent CD36 induction in both HFCD-HF/G groups (Fig. 5C, D). There was a tendency that upregulation of CD36 mRNA level was slightly higher in *Nlrp3*^{-/-} mice than WT mice under HFCD-HF/G feeding, however, no statistical difference was found, which did not support that hepatic CD36 was actually responsible for the worsened NASH pathology in *Nlrp3*^{-/-} mice.

Enhanced hepatic infiltration of iNOS⁺ M1 macrophages with NLRP3 deficiency

Liver macrophages, comprising resident Kupffer cells (KCs) and infiltrating monocyte-derived macrophages (IMDMs), display high degrees of plasticity and heterogeneity [28, 29]. Extensive studies have reported that macrophages shaped by local microenvironment could be broadly divided into two polarized subsets, namely pro-inflammatory M1 and anti-inflammatory M2 macrophages [30]. Under the stress of lipotoxicity, activation of KCs triggers M1-like IMDM recruitment towards liver, intensifying hepatic inflammatory and fibrotic responses [31]. Considering the increased TNF- α and MCP-1 transcription and inflammatory infiltration in the liver of both *Nlrp3*^{-/-} groups compared with corresponding WT group, it was assumable that the macrophages should be involved. Therefore, immunofluorescent staining of liver sections was

Fig. 5 Transcription levels of TNF- α , MCP-1 and CD36 expression in the liver. mRNA levels of TNF- α and MCP-1 in the liver (A) and eWAT (B). C, D Hepatic CD36 expression at mRNA (C) and protein level (D). Protein expression was measured by immunoblotting and quantified by image J.



performed to make a distinction among M1 macrophages with iNOS, M2 macrophages with CD163 and total KCs with its marker CD68 [29]. M1 staining combined with the quantitative analysis demonstrated that HFCD-HF/G feeding led to significantly enhanced expression of CD68 and iNOS in both genotypes of mice compared to control diet, accompanied by an enlarged overlaid area indicating that CD68⁺/iNOS⁺ pro-inflammatory M1-like KCs were remarkably increased. However, iNOS outside KCs that mainly comes from M1-like IMDMs was unexpectedly more distributed in *Nlrp3*^{-/-} groups than respective WT groups (Fig. 6A). M2 staining with its analysis showed that HFCD-HF/G feeding also elevated CD163 expression, which was almost confined to the CD68⁺ fluorescent area, suggesting the simultaneously increased CD68⁺/CD163⁺ M2-like KCs (Fig. 6B). In summary, these results signified that NLRP3 deficiency prompted NASH development under HFCD-HF/G feeding presumably through enhanced hepatic infiltration of iNOS⁺ M1 macrophages.

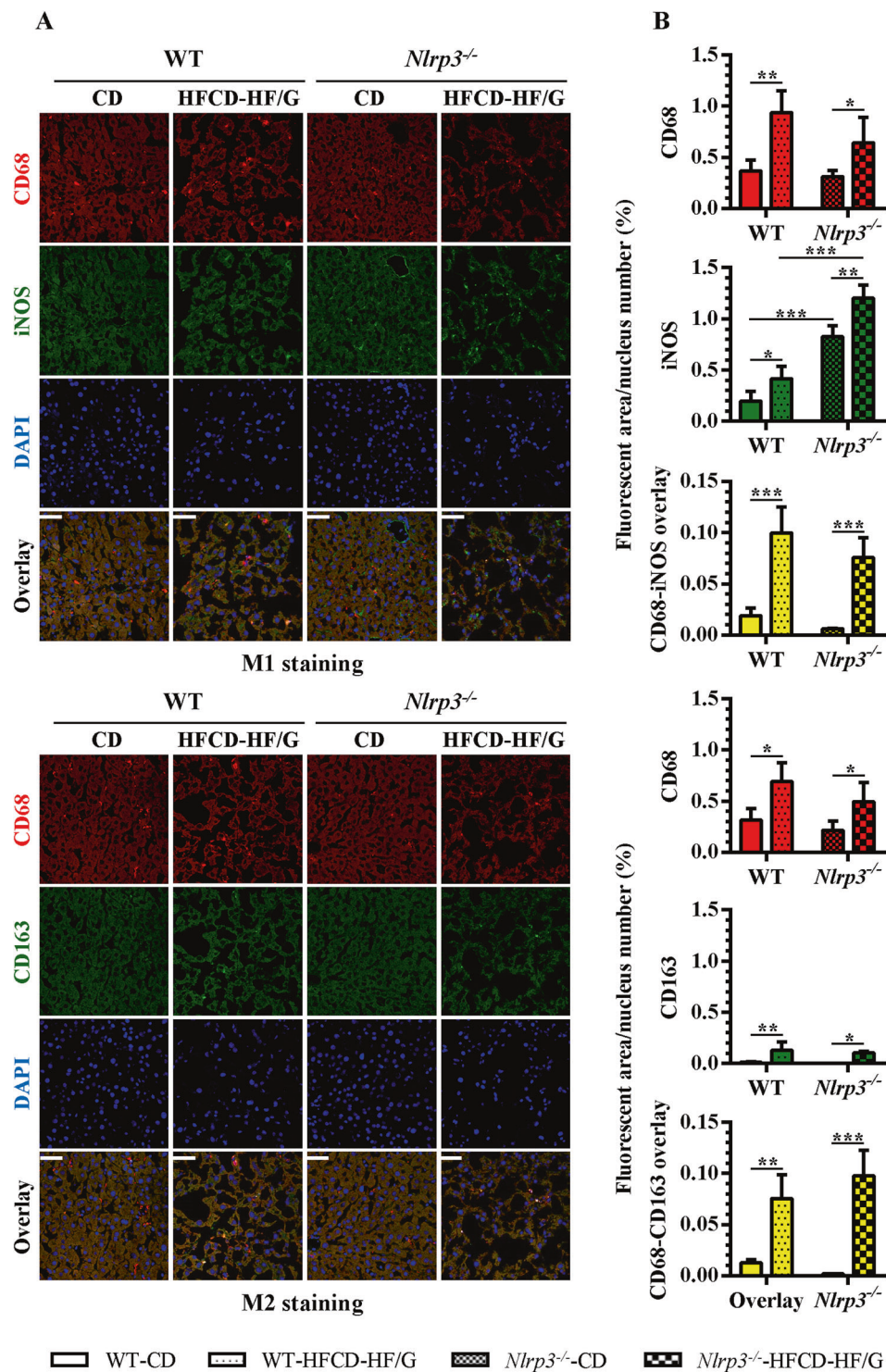
Discussion

A prolonged excess nutrition may trigger NAFLD progression to NASH [22], which could evolve ultimately to cirrhosis causing serious complications including liver failure and HCC. NASH has been shown to develop

through a multifactorial process where nutrition and lifestyle, adipose tissue dysfunction, insulin resistance and chronic inflammation are implicated [7]. NLRP3 is primarily credited with forming inflammasome for sensing endogenous and exogenous dangers and for the subsequent orchestration of inflammatory responses [32]. Aberrant NLRP3 activation is associated with various inflammatory diseases [33–35], and increased NLRP3 expression and downstream pyroptotic activation are well documented in both animal models and NASH patients [13, 14, 20, 36]. While NLRP3 deficiency was reported to suppress fibrosis in a choline-deficient amino acid-defined (CDA) diet-induced murine model of NASH [37], controversial studies argued that NLRP3 deficiency led to a worsened phenotype of NAFLD due to altered gut microbiota [17, 18]. Different animal models used and the complex roles of inflammasome components in regulating intrinsic metabolic and inflammatory responses may offer an explanation for these discrepancies. In fact, NLRP3 is differentially expressed in many cell types although primarily in macrophages [38], and there is mounting evidence regarding its physiological functions in TGF- β receptor signaling [34], T_H2 differentiation [39], catecholamine-dependent lipolysis [40], intestinal barrier [17] and metabolic homeostasis [41]. The present study is designed to further delineate the role of NLRP3 in NASH development by establishing the pathology in NLRP3 knock-out mice using a well-characterized

Fig. 6 Enhanced hepatic infiltration of iNOS⁺ M1 macrophages with NLRP3 deficiency. A, B

Immunofluorescent staining of macrophages was performed on frozen liver sections with Kupffer cell marker CD68 (red) and M1 macrophages marker iNOS (green) (A) or M2 macrophages marker CD163 (green) (B). DAPI (blue) showed the nucleus. Different fluorescent area was quantified using Image J and normalized by nucleus number. Magnification, 400 \times ; Scale bars, 50 μ m.



HFCD-HF/G feeding [20], which has been used to evaluate therapeutic effects of potential agents, such as DHA [24] and Hepalptide [42].

Basic liver NLRP3 expression in WT mice was relatively high compared to eWAT under control diet feeding; whereas more profound NLRP3 expression in response to HFCD-HF/G feeding was noted in eWAT than the liver.

The tissue differential expression of NLRP3 under different diets implied its possible physiological role in healthy liver; while its pro-inflammatory effect may dominate the stressed WAT with excessive nutrient consumption [43, 44]. NLRP3 deficiency prompted more severe HFCD-HF/G-induced obesity and steatohepatitis in *Nlrp3*^{-/-} mice characterized by further elevated body and liver weight, hepatic TG

content and serum ALT level in comparison to WT mice. NAFLD activity score (NAS) was unexpectedly increased in *Nlrp3*^{-/-} mice compared to WT mice under control diet ($p < 0.05$), with major difference coming from the inflammation index. Masson staining demonstrated that hepatic collagen deposition was more evident in *Nlrp3*^{-/-} mice than WT mice especially under HFCD-HF/G feeding. Taken together, NLRP3 deficiency did not alleviate NASH including fibrotic progression but may aggravate manifestations of the disease. The finding of reduced serum TG levels in both *Nlrp3*^{-/-} groups was consistent with Kotas's study, indicating a possible accelerated effect on lipid clearance due to NLRP3 deficiency [45]. From IGTT, we noticed a worsened glucose intolerance in *Nlrp3*^{-/-} mice compared to WT mice under HFCD-HF/G feeding, signifying a more compromised systemic insulin sensitivity occurred in mice with NLRP3 deficiency. Expression of AKT and pAKT-Ser473 was found greatly impaired by HFCD-HF/G in eWAT of both genotypes, however, hepatic pAKT-Ser473 was not significantly affected in *Nlrp3*^{-/-} mice under HFCD-HF/G feeding compared with the control diet. Therefore, NLRP3 deficiency did not ameliorate insulin resistance in the liver, and HFCD-HF/G feeding caused an obvious insulin signaling interruption in eWAT regardless of genotypes. This finding was consistent with unrelieved Western diet-induced adipose tissue inflammation and glucose intolerance in NLRP3 knock-out mice [19]. Meanwhile, it was implied that a fully functional WAT was required to maintain normal glucose level and that insulin resistance might be initiated in adipose tissue [46]. Considering that the AKT signaling is crucial for converging multiple intracellular and extracellular cascades rather than single insulin receptor to regulate diverse cellular processes including inflammation [27, 47], we speculated that the remarkably increased hepatic pAKT-Ser473 in two *Nlrp3*^{-/-} groups compared with WT groups might be linked to altered inflammatory status in the liver.

For in-depth study of NLRP3 in the mediation of inflammatory response, mRNA levels of TNF- α and MCP-1 were determined and found to be further increased in the liver but decreased in eWAT of *Nlrp3*^{-/-} mice compared to WT mice under HFCD-HF/G feeding, implicating that the pro-inflammatory milieu of obese WAT could be mediated at least in part by locally enhanced NLRP3 expression [44]. Moreover, transcription of these genes was even upregulated in both liver and eWAT of control diet-fed *Nlrp3*^{-/-} mice. It was noted that hepatic MCP-1 expression was more remarkable in both *Nlrp3*^{-/-} groups than WT groups. As CD36 has emerged to be a pivotal membrane protein in regulating lipid homeostasis and inflammatory response [48], increased CD36 expression was observed in the liver under HFCD-HF/G feeding, however, no statistical difference between WT and *Nlrp3*^{-/-} mice made it unfavorable to

attribute CD36 for the worsened steatohepatitis with NLRP3 deficiency. The overall enhanced inflammatory status in the liver while lack of NLRP3 prompted us to explore a link to hepatic macrophages. Through immunofluorescent staining, we noted that iNOS and CD163 expression overlaid with CD68 were significantly increased by HFCD-HF/G compared to control diet, indicating that HFCD-HF/G feeding stimulated both pro-inflammatory and anti-inflammatory KCs. However, iNOS beyond KCs was strikingly induced in two *Nlrp3*^{-/-} groups, which suggested a profound infiltration of M1 macrophages towards liver concomitant with NLRP3 deficiency. Given the simultaneously enhanced MCP-1 expression, it might perpetuate the vicious cycle of macrophage recruitment that consequently contributed to the aggravated hepatic inflammatory and fibrotic responses in *Nlrp3*^{-/-} mice [49]. The possibility of compensatory effect by other inflammasomes, such as AIM2 [50], could not be ruled out after NLRP3 deletion, since the inflammasome family consists of multiple members, such as AIM2, NLRP1 and NLRC4. However, from an integrative perspective on the metabolism-inflammation interplay, the impact of NLRP3 deficiency might dominate under HFCD-HF/G feeding based on the evidence that AIM2 did not induce downstream signaling molecules caspase-1 and IL-1 β in response to viral infection in *Nlrp3*^{-/-} mice [51]. Nevertheless, such a phenomenon needs to be further investigated in reliable NASH models to better reflect inflammasome response under metabolic disturbance.

In conclusion, NLRP3 deficiency did not attenuate but aggravate the development of NASH under HFCD-HF/G feeding, including further increased body and liver weight, serum ALT level, systemic insulin resistance, hepatic TG accumulation and collagen deposition. Enhanced inflammatory response in the liver was highlighted by elevated MCP-1 transcription and M1 macrophages infiltration that might account for the worsened NASH pathology in *Nlrp3*^{-/-} mice. The findings reveal that NLRP3 disruption may pose threat to inflammatory regulation, and future research is required to address whether NLRP3 is to become a reliable therapeutic target for the clinical management of NASH.

Acknowledgements The authors are in debt to Associate Prof. Si Zhang in the Dept. of Biochemistry and Molecular Biology for providing the NLRP3 knock-out mice, and Prof. Xiuping Liu in the Dept. Pathology and Laboratory Medicine, School of Basic Medical Sciences, Fudan University for her generous assistance in pathologic evaluation of NAFLD activity score in H&E stained sections. The authors are grateful for technical assistance from the Technology Platform of Fudan University School of Basic Medical Sciences for the use of confocal microscope in this study.

Funding This work is supported by the National Key R&D Program of China (#2016YFE0107400), the National Natural Science Foundation of China (NSFC #81272436, 81572356, 81871997), Shanghai Commission of Sciences and Technologies (#16140903700) to JW.

Author contributions L-YZ: Experimental design and conduct, data collection and analysis, manuscript preparation. CL, Z-RL: participating in experiment conduct and data analysis. CN: technical assistance and supervision. JW: Concept development, experimental design, data analysis, funding support, and manuscript preparation and finalization.

Compliance with ethical standards

Conflict of interest The authors declare that they have no conflict of interest.

Publisher's note Springer Nature remains neutral with regard to jurisdictional claims in published maps and institutional affiliations.

References

- Diehl AM, Day C. Cause, pathogenesis, and treatment of non-alcoholic steatohepatitis. *N Engl J Med*. 2017;377:2063–72.
- Younossi ZM, Koenig AB, Abdelatif D, Fazel Y, Henry L, Wymer M. Global epidemiology of nonalcoholic fatty liver disease—Meta-analytic assessment of prevalence, incidence, and outcomes. *Hepatology*. 2016;64:73–84.
- Wu J. Utilization of animal models to investigate nonalcoholic steatohepatitis-associated hepatocellular carcinoma. *Oncotarget*. 2016;7:42762–76.
- Ye J, Li TS, Xu G, Zhao YM, Zhang NP, Fan J, et al. JCAD promotes progression of nonalcoholic steatohepatitis to liver cancer by inhibiting LATS2 kinase activity. *Cancer Res*. 2017;77:5287–5300.
- Younossi ZM, Otgonsuren M, Henry L, Venkatesan C, Mishra A, Erario M, et al. Association of nonalcoholic fatty liver disease (NAFLD) with hepatocellular carcinoma (HCC) in the United States from 2004 to 2009. *Hepatology*. 2015; 62:1723–30.
- Kleiner DE, Brunt EM, Wilson LA, Behling C, Guy C, Contos M, et al. Association of histologic disease activity with progression of nonalcoholic fatty liver disease. *JAMA Netw Open*. 2019;2: e1912565.
- Tilg H, Moschen AR. Evolution of inflammation in nonalcoholic fatty liver disease: the multiple parallel hits hypothesis. *Hepatology*. 2010;52:1836–46.
- Martinon F, Burns K, Tschopp J. The inflammasome: a molecular platform triggering activation of inflammatory caspases and processing of proIL- β . *Mol Cell*. 2002;10:417–26.
- Schroder K, Tschopp J. The inflammasomes. *Cell*. 2010;140: 821–32.
- Szabo G, Csak T. Inflammasomes in liver diseases. *J Hepatol*. 2012;57:642–54.
- Thomas HNAFLD. A critical role for the NLRP3 inflammasome in NASH. *Nat Rev Gastroenterol Hepatol*. 2017;14:197.
- Wree A, Eguchi A, McGeough MD, Pena CA, Johnson CD, Canbay A, et al. NLRP3 inflammasome activation results in hepatocyte pyroptosis, liver inflammation, and fibrosis in mice. *Hepatology*. 2014;59:898–910.
- Zhang NP, Liu XJ, Xie L, Shen XZ, Wu J. Impaired mitophagy triggers NLRP3 inflammasome activation during the progression from nonalcoholic fatty liver to nonalcoholic steatohepatitis. *Lab Invest*. 2019;99:749–63.
- Gaul S, Leszczynska A, Alegre F, Kaufmann B, Johnson CD, Adams LA, et al. Hepatocyte pyroptosis and release of inflammasome particles induce stellate cell activation and liver fibrosis. *J Hepatol*. 2021;74:156–67.
- Duan NN, Liu XJ, Wu J. Palmitic acid elicits hepatic stellate cell activation through inflammasomes and hedgehog signaling. *Life Sci*. 2017;176:42–53.
- Mridha AR, Wree A, Robertson AAB, Yeh MM, Johnson CD, Van Rooyen DM, et al. NLRP3 inflammasome blockade reduces liver inflammation and fibrosis in experimental NASH in mice. *J Hepatol*. 2017;66:1037–46.
- Henao-Mejia J, Elinav E, Jin C, Hao L, Mehal WZ, Strowig T, et al. Inflammasome-mediated dysbiosis regulates progression of NAFLD and obesity. *Nature*. 2012;482:179–85.
- Pierantonelli I, Rychlicki C, Agostinelli L, Giordano DM, Gaggini M, Fraumene C, et al. Lack of NLRP3-inflammasome leads to gut-liver axis derangement, gut dysbiosis and a worsened phenotype in a mouse model of NAFLD. *Sci Rep*. 2017;7:12200.
- Ringling RE, Gastecki ML, Woodford ML, Lum-Naihe KJ, Grant RW, Pulakat L, et al. Loss of Nlrp3 does not protect mice from western diet-induced adipose tissue inflammation and glucose intolerance. *PLoS One*. 2016;11:e0161939.
- Liu XJ, Duan NN, Liu C, Niu C, Liu XP, Wu J. Characterization of a murine nonalcoholic steatohepatitis model induced by high fat high calorie diet plus fructose and glucose in drinking water. *Lab Invest*. 2018;98:1184–99.
- Wree A, Kahraman A, Gerken G, Canbay A. Obesity affects the liver - the link between adipocytes and hepatocytes. *Digestion*. 2011;83:124–33.
- Caputo T, Gilardi F, Desvergne B. From chronic overnutrition to metaflammation and insulin resistance: adipose tissue and liver contributions. *FEBS Lett*. 2017;591:3061–88.
- Kleiner DE, Brunt EM, Van Natta M, Behling C, Contos MJ, Cummings OW, et al. Design and validation of a histological scoring system for nonalcoholic fatty liver disease. *Hepatology*. 2005;41:1313–21.
- Liu X-J, Xie L, Du K, Liu C, Zhang N-P, Gu C-J, et al. Succinate-GPR-91 receptor signalling is responsible for nonalcoholic steatohepatitis-associated fibrosis: Effects of DHA supplementation. *Liver Int*. 2020;40:830–43.
- Ino H. Antigen retrieval by heating en bloc for pre-fixed frozen material. *J Histochem Cytochem*. 2003;51:995–1003.
- Yamashita S, Okada Y. Application of heat-induced antigen retrieval to aldehyde-fixed fresh frozen sections. *J Histochem Cytochem*. 2005;53:1421–32.
- Manning BD, Toker A. AKT/PKB signaling: navigating the network. *Cell*. 2017;169:381–405.
- Morinaga H, Mayoral R, Heinrichsdorff J, Osborn O, Franck N, Hah N, et al. Characterization of distinct subpopulations of hepatic macrophages in HFD/obese mice. *Diabetes*. 2015;64:1120–30.
- Krenkel O, Tacke F. Liver macrophages in tissue homeostasis and disease. *Nat Rev Immunol*. 2017;17:306–21.
- Kazankov K, Jorgensen SMD, Thomsen KL, Moller HJ, Vilstrup H, George J, et al. The role of macrophages in nonalcoholic fatty liver disease and nonalcoholic steatohepatitis. *Nat Rev Gastroenterol Hepatol*. 2019;16:145–59.
- Krenkel O, Puengel T, Govaere O, Abdallah AT, Mossanen JC, Kohlhepp M, et al. Therapeutic inhibition of inflammatory monocyte recruitment reduces steatohepatitis and liver fibrosis. *Hepatology*. 2018;67:1270–83.
- Prochnicki T, Latz E. Inflammasomes on the crossroads of innate immune recognition and metabolic control. *Cell Metab*. 2017;26:71–93.
- Lee HM, Kim JJ, Kim HJ, Shong M, Ku BJ, Jo EK. Upregulated NLRP3 inflammasome activation in patients with type 2 diabetes. *Diabetes*. 2013;62:194–204.
- Lech M, Lorenz G, Kulkarni OP, Grosser MO, Stigrot N, Darisipudi MN, et al. NLRP3 and ASC suppress lupus-like

- autoimmunity by driving the immunosuppressive effects of TGF-beta receptor signalling. *Ann Rheum Dis*. 2015;74:2224–35.
35. Osuka A, Hanschen M, Stoecklein V, Lederer JA. A protective role for inflammasome activation following injury. *Shock*. 2012;37:47–55.
 36. Kim SH, Kim G, Han DH, Lee M, Kim I, Kim B, et al. Ezetimibe ameliorates steatohepatitis via AMP activated protein kinase-TFEB-mediated activation of autophagy and NLRP3 inflammasome inhibition. *Autophagy*. 2017;13:1767–81.
 37. Wree A, McGeough MD, Pena CA, Schlattjan M, Li H, Inzaugarat ME, et al. NLRP3 inflammasome activation is required for fibrosis development in NAFLD. *J Mol Med (Berl)*. 2014;92:1069–82.
 38. Guarda G, Zenger M, Yazdi AS, Schroder K, Ferrero I, Menu P, et al. Differential expression of NLRP3 among hematopoietic cells. *J Immunol*. 2011;186:2529–34.
 39. Bruchard M, Rebe C, Derangere V, Togbe D, Ryffel B, Boidot R, et al. The receptor NLRP3 is a transcriptional regulator of TH2 differentiation. *Nat Immunol*. 2015;16:859–70.
 40. Camell CD, Sander J, Spadaro O, Lee A, Nguyen KY, Wing A, et al. Inflammasome-driven catecholamine catabolism in macrophages blunts lipolysis during ageing. *Nature*. 2017;550:119–23.
 41. Jiang D, Chen S, Sun R, Zhang X, Wang D. The NLRP3 inflammasome: Role in metabolic disorders and regulation by metabolic pathways. *Cancer Lett*. 2018;419:8–19.
 42. Liu XJ, Liu C, Zhu LY, Fan CL, Niu C, Liu XP, et al. Hepalptide ameliorated progression of nonalcoholic steatohepatitis in mice. *Biomed Pharmacother*. 2020;126:110053.
 43. Prakash S, Rai U, Kosuru R, Tiwari V, Singh S. Amelioration of diet-induced metabolic syndrome and fatty liver with sitagliptin via regulation of adipose tissue inflammation and hepatic Adiponectin/AMPK levels in mice. *Biochimie*. 2020;168:198–209.
 44. Vandanmagsar B, Youm YH, Ravussin A, Galgani JE, Stadler K, Mynatt RL, et al. The NLRP3 inflammasome instigates obesity-induced inflammation and insulin resistance. *Nat Med*. 2011;17:179–88.
 45. Kotas ME, Jurczak MJ, Annicelli C, Gillum MP, Cline GW, Shulman GI, et al. Role of caspase-1 in regulation of triglyceride metabolism. *Proc Natl Acad Sci USA*. 2013;110:4810–5.
 46. Smith U. Impaired ('diabetic') insulin signaling and action occur in fat cells long before glucose intolerance—is insulin resistance initiated in the adipose tissue? *Int J Obes Relat Metab Disord*. 2002;26:897–904.
 47. Vergadi E, Ieronymaki E, Lyroni K, Vaporidi K, Tsatsanis C. Akt Signaling Pathway in Macrophage Activation and M1/M2 Polarization. *J Immunol*. 2017;198:1006–14.
 48. Zhong S, Zhao L, Wang Y, Zhang C, Liu J, Wang P, et al. Cluster of differentiation 36 deficiency aggravates macrophage infiltration and hepatic inflammation by upregulating monocyte chemoattractant protein-1 expression of hepatocytes through histone deacetylase 2-dependent pathway. *Antioxid Redox Signal*. 2017;27:201–14.
 49. Schuster S, Cabrera D, Arrese M, Feldstein AE. Triggering and resolution of inflammation in NASH. *Nat Rev Gastroenterol Hepatol*. 2018;15:349–64.
 50. Sun L, Ma W, Gao W, Xing Y, Chen L, Xia Z, et al. Propofol directly induces caspase-1-dependent macrophage pyroptosis through the NLRP3-ASC inflammasome. *Cell Death Dis*. 2019;10:542.
 51. de Castro-Jorge LA, de Carvalho RVH, Klein TM, Hiroki CH, Lopes AH, Guimaraes RM, et al. The NLRP3 inflammasome is involved with the pathogenesis of Mayaro virus. *PLoS Pathog*. 2019;15:e1007934.